NONLINEAR DYNAMICS AND ADAPTIVE CONTROL USING THE DYNAMIC INVERSION CONCEPT AND NEURAL NETWORKS FOR A GUIDANCE GYROSYSTEM (GG) WITH ONE GYROSCOPE AND TWO SUSPENSION GIMBALS (GAR) PART 2. ADAPTIVE CONTROL ARHITECTURE DESING AND VALIDATION

Constantin Adrian MIHAI[*], Romulus LUNGU[*,]**

[*]Politehnica University of Bucharest, Doctoral School of Aerospace Engineering, Bucharest, Romania
(adrianmihai10.07@gmail.com)
[**]Member IAA – International Academy Astronautics, Paris, France
(romulus_lungu@yahoo.com)

DOI: 10.19062/2247-3173.2025.26.19

Abstract: *This paper presents the design of the adaptive control system of GG with GAR, consisting of a stabilization controller and an orientation controller; the concept of dynamic inversion is used. The equations of nonlinear dynamics of GG were obtained in Part 1 of this paper series.The stabilization controller (for the stabilization mode) consists of a 2nd order reference model, a linear dynamic compensator, of the P.D type, a linear state observer and a neural network. The neural network models the adaptive component of the control law, which has the role of compensating for the dynamic inversion error. The orientation controller is chosen as P.I. type. In stabilization mode, the system compensates for the effect of external disturbances induced by the rotations of the base (rocket), and in orientation mode, the system controls the rotation of the target coordinator TC so that the sighting line (TC axis) overlaps the guidance line. By numerical simulations, using the Matlab/Simulink model, the dynamic characteristics of GG are drawn for the stabilization mode and for the orientation mode.*

Keyords*: stabilization, guidance, dynamic inversion, neural network*

1. INTRODUCTION

The automatic control of the dynamics of gyroscopic systems for orientation and stabilization mono, bi and triaxial is addressed in many specialized works. In most of these, linearized dynamic models are used, with linear control laws, as for example, in the papers [1-7]. It is also worth mentioning the works in which the control laws used are nonlinear [8-18]. Nonlinear models and nonlinear control laws can be used for gyrosystems with GAR obtained by particularizing those deduced for DGMSCMG [19-22].

In this article, adaptive control based on the concept of dynamic inversion and the use of neural networks is used [23-26]. The controllers used for the orientation mode are of the P.I. or P.I.D. type, while those for the stabilization mode have linear dynamic compensators, linear state observers and neural networks as components. The neural network models the adaptive component of the control law, having the role, through its effect, to compensate for the influence of the dynamic inversion error.

The design of the two controllers is done in Section 2. Section 3 presents the Matlab Simulink model and, with it, the GG characteristics for the stabilization mode and for the orientation mode are plotted. In Section 4, conclusions are formulated.

2. DESIGN OF ADAPTIVE CONTROL SYSTEM OF GG WITH GAR

The concept of dynamic inversion and a neural network [23,24] are used to model the adaptive component, which has the role of compensating for the dynamic inversion error $\boldsymbol{\varepsilon} = [\varepsilon_1 \ \varepsilon_2]^T$.

Choosing output variables $y_1 = \omega_{g1}, y_2 = \omega_{g2}$ and input variables $u_1 = i_y$ and $u_2 = i_x$, equations (22) (from Part 2 of this paper series) can be expressed as follows

$$\ddot{y}_1 = v_1 = \hat{v}_1 + \varepsilon_1,\ \ddot{y}_2 = v_2 = \hat{v}_2 + \varepsilon_2;\ \hat{v}_1 = \hat{h}_{r1}(\boldsymbol{y}, \hat{\boldsymbol{u}}),\ \hat{v}_2 = \hat{h}_{r2}(\boldsymbol{y}, \hat{\boldsymbol{u}}); \tag{1}$$

ε_1 and ε_2 (dynamic inversion errors) contain all the other terms in (22)-from Part 1 of this paper series.

With the notations

$$m_1 = -\frac{f_y - (a_3 + b_1)\omega_{t2}}{b_0}, m_2 = \frac{\omega_{x_T}(\omega_{t1} + \omega_{x_T}\sin^2\lambda_2^*)}{b_0}, m_3 = \frac{r_1}{r_2}\frac{\cos^2\lambda_2^*(b_1 - a_1)\omega_{x_T}}{b_0},$$

$$m_4 = r_1\frac{a_3 + b_1}{b_0}(\omega_{t1} + \omega_{x_T}\omega_{t1} + \dot{\omega}_{x_T}), m_5 = \frac{a_3 + b_1}{r_2 b_0} + \omega_{x_T}^2, m_6 = \frac{a_3 + b_1}{r_1 b_0}, m_7 = \frac{a_0}{r_2 b_0}\omega_{t2},$$

$$m_8 = \frac{r_1(a_3 + b_1)}{r_2^2 b_0}\dot{\omega}_{x_T}, m_9 = \frac{a_3 + b_1}{r_1}, m_{10} = \frac{\omega_{x_T}}{r_1 r_2 b_0}, m_{11} = \frac{a_0 - r_1 c}{r_2^2 b_0}, m_{12} = \frac{r_1 k_y}{b_0 K}, \tag{2}$$

$$n_1 = \frac{f_x}{a_0}, n_2 = \frac{\omega_{x_T}}{a_0}, n_3 = \frac{r_2}{r_1}\frac{1 - d_0\omega_{x_T}}{a_0}, n_4 = \frac{r_2}{r_1}\frac{a_0\dot{\omega}_{x_T} + f_x\omega_{x_T}}{a_0}\frac{r_2}{r_1}, n_5 = \frac{c + c_1}{r_1 a_0}(\omega_{t1} + \omega_Y),$$

$$n_6 = \frac{e_0}{r_1^2 a_0}, n_7 = \frac{e_0\omega_{x_T}}{r_1 r_2 a_0}, n_8 = \frac{r_2 k_x}{a_0 K},$$

the following results

$$\hat{v}_1 = \hat{h}_{r1}(\boldsymbol{y}, \hat{\boldsymbol{u}}) = -m_2 y_1 - m_4 y_2 + m_5 y_1 y_2 - m_{12} i_y; \tag{3}$$

$$\hat{v}_2 = \hat{h}_{r2}(\boldsymbol{y}, \hat{\boldsymbol{u}}) = -n_4 y_1 - n_2 y_2 + n_8 i_x; \tag{4}$$

$$\boldsymbol{\varepsilon}_1 = -m_1\hat{\dot{y}}_1 - m_3\hat{\dot{y}}_2 + m_6 y_1\hat{\dot{y}}_1 - m_7\hat{\dot{y}}_1 y_1 - m_8 y_2\hat{\dot{y}}_2 - m_9 y_1\hat{\dot{y}}_2 - m_{10} y_1\hat{\dot{y}}_1 y_2 + m_{11}\hat{\dot{y}}_1 y_2\hat{\dot{y}}_2 + N_y^*/b_0 \tag{5}$$

$$\boldsymbol{\varepsilon}_2 = n_3\hat{\dot{y}}_1 - n_1\hat{\dot{y}}_2 + n_5\hat{\dot{y}}_1 y_1 - n_6\hat{\dot{y}}_1^2 y_2 - n_7\hat{\dot{y}}_1 y_2\hat{\dot{y}}_2 + N_x^*/a_0 \tag{6}$$

The variables $\hat{\dot{y}}_1$ and $\hat{\dot{y}}_2$ represent the estimates of the variables $\dot{y}_1$ and $\dot{y}_2$, components of the output vector of the state observer.

The previous equations can be expressed in vector form

$$\ddot{\boldsymbol{y}} = \hat{\boldsymbol{v}} + \boldsymbol{\varepsilon}, \ddot{\boldsymbol{y}} = [\ddot{y}_1 \ \ddot{y}_2]^T, \hat{\boldsymbol{v}} = [\hat{v}_1 \ \hat{v}_2]^T, \boldsymbol{\varepsilon} = [\varepsilon_1 \ \varepsilon_2]^T, \tag{7}$$

$$\hat{\boldsymbol{v}} = \hat{\boldsymbol{h}}_r(\boldsymbol{y}, \hat{\boldsymbol{u}}) = \begin{bmatrix} \hat{h}_{r1}(\boldsymbol{y}, \hat{\boldsymbol{u}}) \\ \hat{h}_{r2}(\boldsymbol{y}, \hat{\boldsymbol{u}}) \end{bmatrix} = -\begin{bmatrix} m_2 & m_4 \\ n_2 & n_4 \end{bmatrix} \boldsymbol{y} + \begin{bmatrix} m_5 \\ 0 \end{bmatrix} y_1 y_2 + \begin{bmatrix} -m_{12} & 0 \\ 0 & n_8 \end{bmatrix} \hat{\boldsymbol{u}} \tag{8}$$

$$\boldsymbol{\varepsilon} = \begin{bmatrix} \boldsymbol{\varepsilon}_1 \\ \boldsymbol{\varepsilon}_2 \end{bmatrix} = \begin{bmatrix} -m_1 \hat{\dot{y}}_1 - m_3 \hat{\dot{y}}_2 + m_6 y_1 \hat{\dot{y}}_1 - m_7 \hat{\dot{y}}_1 y_1 - m_8 y_2 \hat{\dot{y}}_2 - m_9 y_1 \hat{\dot{y}}_2 - m_{10} y_1 \hat{\dot{y}}_1 y_2 + m_{11} \hat{\dot{y}}_1 y_2 \hat{\dot{y}}_2 + N_y^* / b_0 \\ n_3 \hat{\dot{y}}_1 - n_1 \hat{\dot{y}}_2 + n_5 \hat{\dot{y}}_1 y_1 - n_6 \hat{\dot{y}}_1^2 y_2 - n_7 \hat{\dot{y}}_1 y_2 \hat{\dot{y}}_2 + N_x^* / a_0 \end{bmatrix} \tag{9}$$

The inverse dynamics, obtained from (8), is described by the equation

$$\hat{\boldsymbol{u}} = \begin{bmatrix} \hat{\boldsymbol{u}}_1 \\ \hat{\boldsymbol{u}}_2 \end{bmatrix} = \begin{bmatrix} \hat{i}_y \\ \hat{i}_x \end{bmatrix} = \hat{\boldsymbol{h}}_r^{-1}(\boldsymbol{y}, \hat{\boldsymbol{v}}) = \begin{bmatrix} -m_{12} & 0 \\ 0 & n_8 \end{bmatrix}^{-1} (\hat{\boldsymbol{v}} + \begin{bmatrix} m_2 & m_4 \\ m_2 & n_4 \end{bmatrix} \boldsymbol{y} - \begin{bmatrix} m_5 \\ 0 \end{bmatrix} y_1 y_2) \tag{10}$$

In Fig. 1.a. the structure of the adaptive control system of the GG is given. Since the relative degrees of the components of the output vector are equal to 2 according to [25], a reference model of order 2 is chosen, having the transfer matrix

$$H_m(s) = \frac{\omega_0^2}{\mathrm{s}^2 + 2\xi\omega_0 \mathrm{s} + \omega_0^2} I_2 \tag{11}$$

The linear dynamic compensator of the stabilization subsystem and, respectively, the orientation controller are chosen as P.D and P.I types, with the transfer matrices

$$H_{gg}(\mathrm{s}) = K_p + K_d \mathrm{s},\ K_p = k_p I_2, K_d = k_d I_2, \tag{12}$$

$$H_o(\mathrm{s}) = K_{p0} + \frac{K_{i0}}{\mathrm{s}},\ K_{p0} = k_{p0} I_2, K_{i0} = k_{i0} I_2, \tag{13}$$

with I_2 - unity matrix (2×2).

The output of the linear dynamic compensator is

$$\hat{\boldsymbol{v}}_{pd} = K_p \tilde{\boldsymbol{y}} + K_d \dot{\tilde{\boldsymbol{y}}} = D_c \boldsymbol{e}, D_c = [K_p\ K_d] = [k_p I_2\ k_d I_2] \tag{14}$$

$$\boldsymbol{e} = [\tilde{\boldsymbol{y}}^T\ \dot{\tilde{\boldsymbol{y}}}^T] = [\boldsymbol{e}_1^T\ \boldsymbol{e}_2^T]^T, \tilde{\boldsymbol{y}} = \bar{\boldsymbol{y}} - \boldsymbol{y},\ \tilde{\boldsymbol{y}} = [\tilde{y}_1\ \tilde{y}_2]^T = [(\bar{y}_1 - y_1)(\bar{y}_2 - y_2)]^T, \dot{\tilde{\boldsymbol{y}}} = [\dot{\tilde{y}}_1\ \dot{\tilde{y}}_2]^T = [(\dot{\bar{y}}_1 - \dot{y}_1)(\dot{\bar{y}}_2 - \dot{y}_2)]^T, \tag{15}$$

Equation $\ddot{\boldsymbol{y}} = \boldsymbol{v} + \boldsymbol{\varepsilon}$ with $\hat{\boldsymbol{v}} = \hat{\boldsymbol{v}}_{pd} + \ddot{\bar{\boldsymbol{y}}} - \hat{\boldsymbol{v}}_a$ (according to Fig.1.a) and $\hat{\boldsymbol{v}}_{pd}$ of the form (14), becomes

$$\ddot{\tilde{\boldsymbol{y}}} = -K_p \tilde{\boldsymbol{y}} - K_d \dot{\tilde{\boldsymbol{y}}} + (\hat{\boldsymbol{v}}_a - \boldsymbol{\varepsilon}) \tag{16}$$

equivalent to the system of equations of state

$$\begin{aligned} \dot{\boldsymbol{e}}_1 &= \boldsymbol{e}_2 \\ \dot{\boldsymbol{e}}_2 &= -K_p \boldsymbol{e}_1 - K_d \boldsymbol{e}_2 + (\hat{\boldsymbol{v}}_a - \boldsymbol{\varepsilon}) \end{aligned} \tag{17}$$

respectively with the equation of state of the linear subsystem with the input $(\hat{\boldsymbol{v}}_a - \boldsymbol{\varepsilon})$ and the output $\tilde{\boldsymbol{y}}$,

$$\dot{\boldsymbol{e}} = A\boldsymbol{e} + B(\hat{\boldsymbol{v}}_a - \boldsymbol{\varepsilon}) \tag{18}$$

in wich

$$A=\begin{bmatrix} 0_{2\times 2} & I_2 \\ -K_p & -K_d \end{bmatrix}_{(4\times 4)},\ B=\begin{bmatrix} 0_{2\times 2} \\ I_2 \end{bmatrix}_{(4\times 2)} \tag{19}$$

The equation of state of the linear observer is [9]

$$\dot{\hat{\boldsymbol{e}}}=A\hat{\boldsymbol{e}}+L(\tilde{\boldsymbol{y}}-\hat{\tilde{\boldsymbol{y}}}) \tag{20}$$

with L-amplification matrix (4×2) and $\hat{\boldsymbol{e}},\hat{\tilde{\boldsymbol{y}}}$ – vector estimates of $\boldsymbol{e},\tilde{\boldsymbol{y}}$

$$\tilde{\boldsymbol{y}}=\boldsymbol{e}_1=C\boldsymbol{e},\hat{\tilde{\boldsymbol{y}}}=\hat{\boldsymbol{e}}_1=C\hat{\boldsymbol{e}},C=[I_2\ 0_{2\times 2}]_{(4\times 2)} \tag{21}$$

With (20), equation (21) becomes

$$\dot{\hat{\boldsymbol{e}}}=\bar{A}\hat{\boldsymbol{e}}+L,\bar{A}=A-LC \tag{22}$$

The amplification matrix L is chosen so that the matrix $\bar{A}$ has its eigen values located in the left complex half-plane (the matrix $\bar{A}$ is asymptotically stable).

The training vector of the neural network NNc is [23]

$$\bar{\boldsymbol{e}}=\hat{\boldsymbol{e}}^T PB \tag{23}$$

with P – matrix (4×4), solution of the Lyapunov equation.

$$\bar{A}^T P+P\bar{A}=-Q \tag{24}$$

with Q – positive definite matrix (4×4).

The adaptive command is calculated with the formula [25]

$$\hat{\boldsymbol{v}}_a=W^T(V^T\eta) \tag{25}$$

W and V the NNc weights, solutions of the system of differential equations of the forms (27), and η is the NNc driving vector, of the form (33) from [20], σ' is the derivative of the sigmoidal function $\sigma(z)=\sigma(V^T\eta)$;

$$\begin{aligned} \dot{W}&=-S_W[2(\sigma-\sigma' V^T\eta)\bar{\boldsymbol{e}}+k(W-W_0)],W_0=W(0) \\ \dot{V}&=-S_V[2\sigma\bar{\boldsymbol{e}}W^T\sigma'+k(V-V_0)],V_0=V(0) \end{aligned} \tag{26}$$

The inner (stabilizing) contour has the transfer matrix of the form

$$H_s(\mathrm{s})=\frac{1}{\mathrm{s}^2+k_d\mathrm{s}+k_p}I_2 \tag{27}$$

and the outer (orientation) contour has the transfer matrix

$$H_c(\mathrm{s})=\frac{k_{p0}\mathrm{s}+k_{i0}}{\mathrm{s}^3+k_d\mathrm{s}^2+(k_{p0}+k_p)\mathrm{s}+k_{i0}}I_2 \tag{28}$$

To calculate the coefficients k_{i0} and k_{p0}, the roots of the characteristic equation are required

$$\mathrm{s}^3+k_d\mathrm{s}^2+(k_{p0}+k_p)\mathrm{s}+k_{i0}=0 \tag{29}$$

in the left complex half-plane.

In order not to use sensors to measure angular velocities $\dot{y}_1=\dot{\omega}_{g1}$ and $\dot{y}_2=\dot{\omega}_{g2}$, in the calculation relationship of inversion errors $\boldsymbol{\varepsilon}$(9) their estimated values are used $\hat{\dot{y}}_1$ and $\hat{\dot{y}}_2$,components of the estimated state vector $\hat{\boldsymbol{e}}_2=\hat{\dot{\boldsymbol{y}}}=[\hat{\dot{y}}_1\ \hat{\dot{y}}_2]^T$. Thus, from (16),

$$\tilde{\boldsymbol{y}} = \boldsymbol{e}_2 = \dot{\bar{\boldsymbol{y}}} - \dot{\boldsymbol{y}} \tag{30}$$

And and for the estimated vector $\hat{\tilde{\boldsymbol{y}}}$ the calculation relationship is

$$\hat{\tilde{\boldsymbol{y}}} = \hat{\boldsymbol{e}}_2 = \dot{\bar{\boldsymbol{y}}} - \dot{\hat{\boldsymbol{y}}} \tag{31}$$

From (31) it follows

$$\hat{\tilde{\boldsymbol{y}}} = \dot{\bar{\boldsymbol{y}}} - \hat{\boldsymbol{e}}_2 = \dot{\bar{\boldsymbol{y}}} - [0_{2\times 2}\ I_2]\hat{\boldsymbol{e}} = \dot{\bar{\boldsymbol{y}}} - Mat\_3\hat{\boldsymbol{e}} \tag{32}$$

with $Mat\_3 = [0_{2\times 2}\ I_2]$.

3. NUMERICAL SIMULATIONS

In Fig.2 the Matlab/Simulink model of the system in Fig.1 is presented.

The following values were chosen: A=B=0.008 N×m×s^2/rad , $A_1 = 0.02$N×m×s^2/rad , $A_1 = 0.02$N×m×s^2/rad , $B_1 = 0.01$N×m×s^2/rad , $C_1 = 0.02$N×m×s^2/rad , $A_2 = 0.58$ N×m ×s^2/rad, $B_2 = 0.02$ N×m×s^2/rad, $C_2 = 0.45$ N×m×s^2/rad, $A_0 = 0.02$ N×m×s^2/rad, B_0 = = 0.66 N×m×s^2/rad, $D_0 = 0.01$ N×m×s^2/rad, $K = 2.5$N×m×s , $F_x = 0.1$N×m×s/rad, $F_y = 0.1$ N×m×s/rad, $\lambda_1^* = 0.52$ rad, $\lambda_2^* = 1$ rad, $\omega_{t1} = 0.2$ rad/s, $\omega_{t2} = 0.15$ rad/s, $\dot{\omega}_{t1}$ = 0 rad/s^2, $\dot{\omega}_{t2} = 0$ rad/s^2, $\omega_{x_T} = 0.15$ rad/s^2, $\dot{\omega}_{x_T} = 0$ rad/s^2, $\omega_X = 0.33$ rad/s, $\omega_Y = 0.05$ rad/s, $\omega_Z = 0.05$ rad /s, $\omega_{g1}(0) = \omega_{g2}(0) = 0.05$ rad/s, $\dot{\omega}_{g1}(0) = \dot{\omega}_{g2}(0) = 0$ rad/s^2, f_x = 0.004 rad^{-1}, $a_3 = 0.32$ s, $f_y = 0.004$ rad^{-1}, $a_1 = 0.08$ s, $a_2 = 0.232$ s, $b_0 = 0.264$ s, $b_1 = 0.004$s, $b_2 = 0.16$s, $c = 0.036$s, $c_1 = 0.004$s, $c_2 = 0.232$s, $d_0 = 0.04$s, $e_0 = 0.004$s, $r_2 = r\cos\lambda_2^* = 0.59$s^{-1}, $r_1 = r = \omega_{t1maximum} / \alpha_{maximum} = 1.18$s^{-1}, $k_x = 1$N×m×A, $k_y = 0.2$ N×m×A, $k_p = 6$s^2.

For NNc the following values were chosen:

$Q_1 = I_4$ (unit matrix),

$d = 0.1, k = 20$, Sv = Sw = 0.01, $b_w = 1$, ,

$W_0 = 0_{11\times 1}, V_0 = 0_{10\times 10}$, $n_1 = 9$ neurons, $n_2 = 10$ neurons, $n_3 = 2$ neurons,

$a_j = [1\ \ 0.9\ \ 0.8\ \ 0.7\ \ 0.6\ \ 0.5\ \ 0.4\ \ 0.3\ \ 0.2\ \ 0.1]$,

With these values, the dynamic characteristics in Fig.3 were constructed.

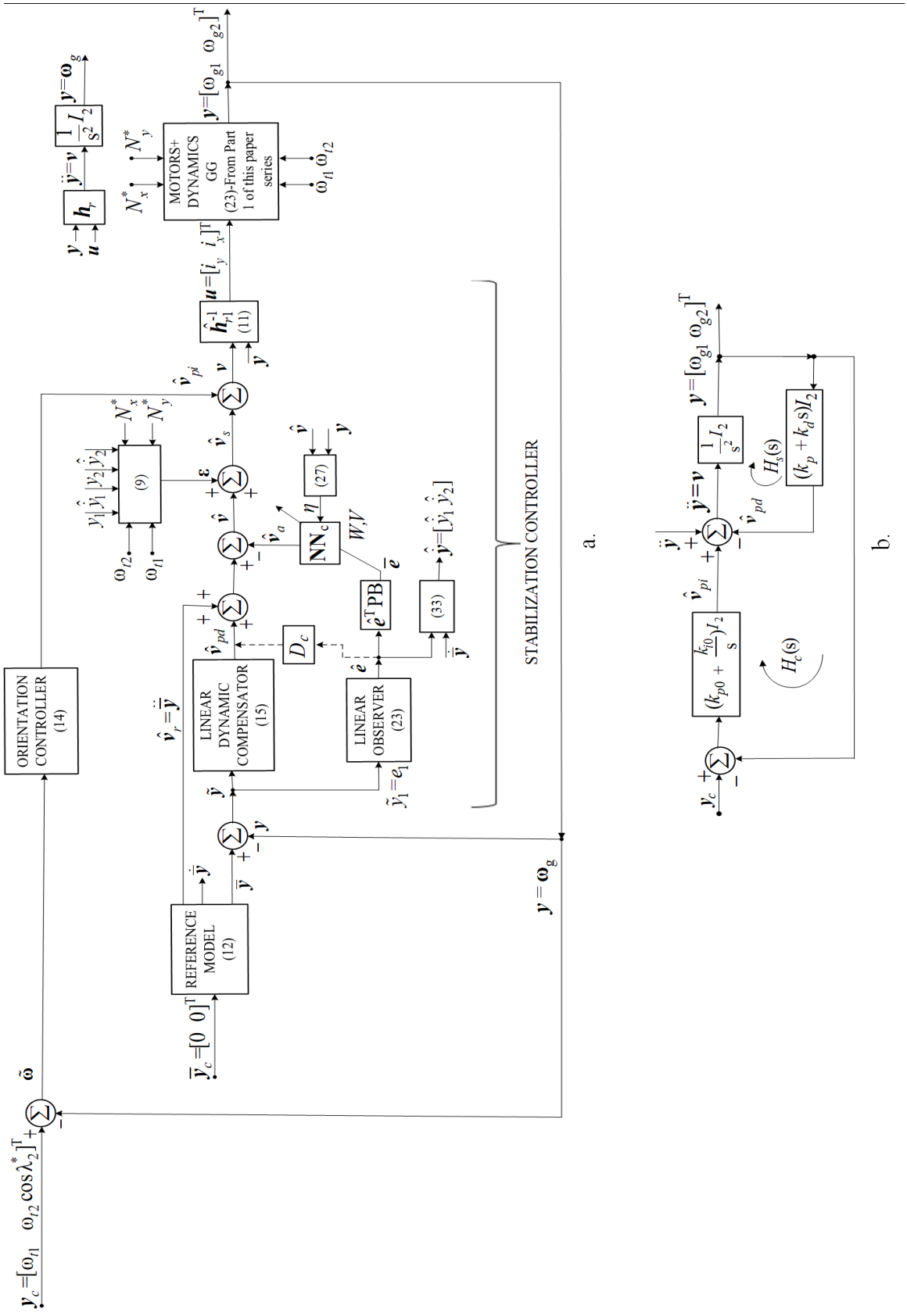

FIG.1 Adaptive control system of nonlinear dynamics of GG: a) complete block diagram; b) block diagram of the linear subsystem

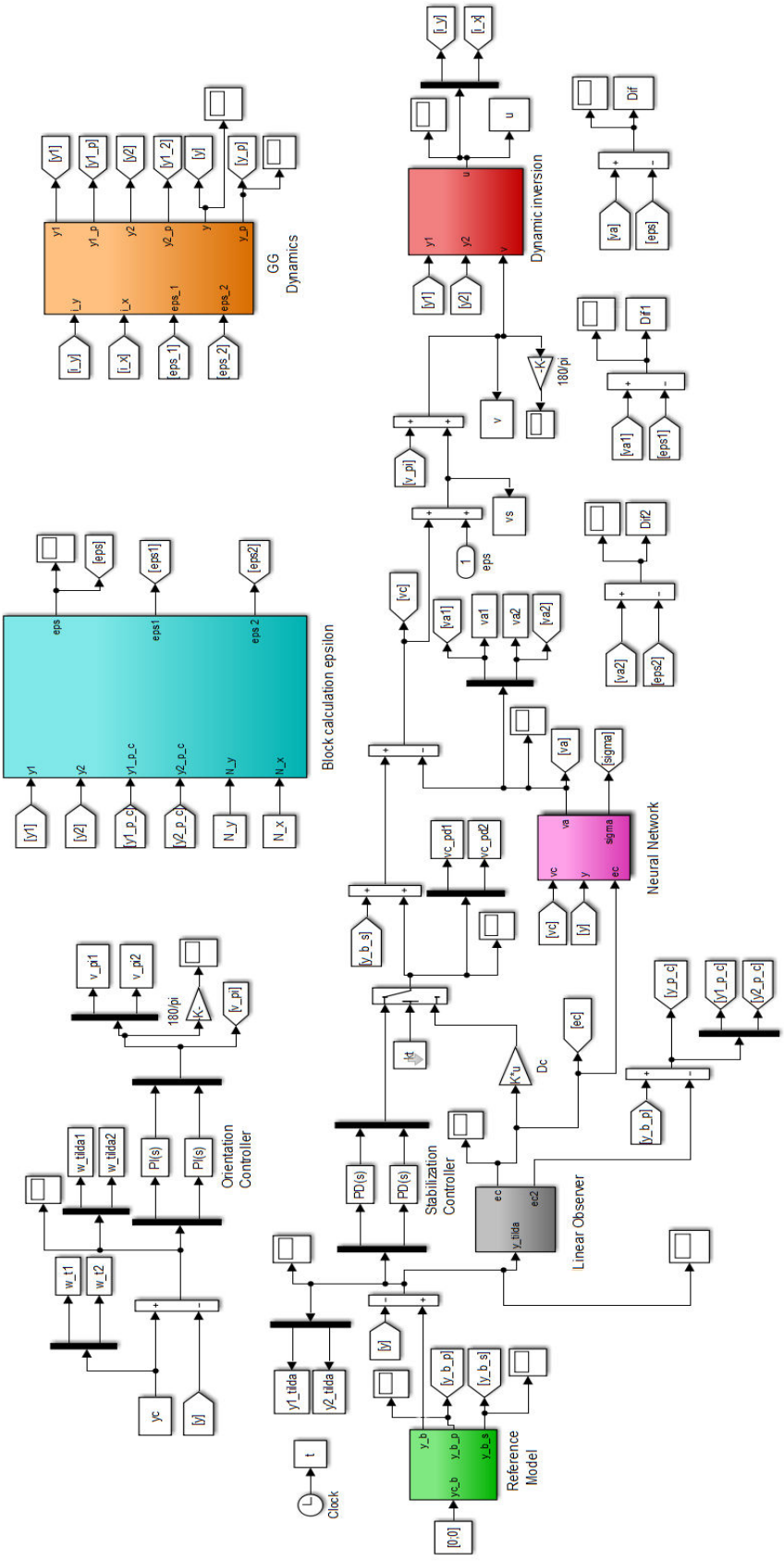

FIG.2 Matlab/Simulink model of the system in Fig.1

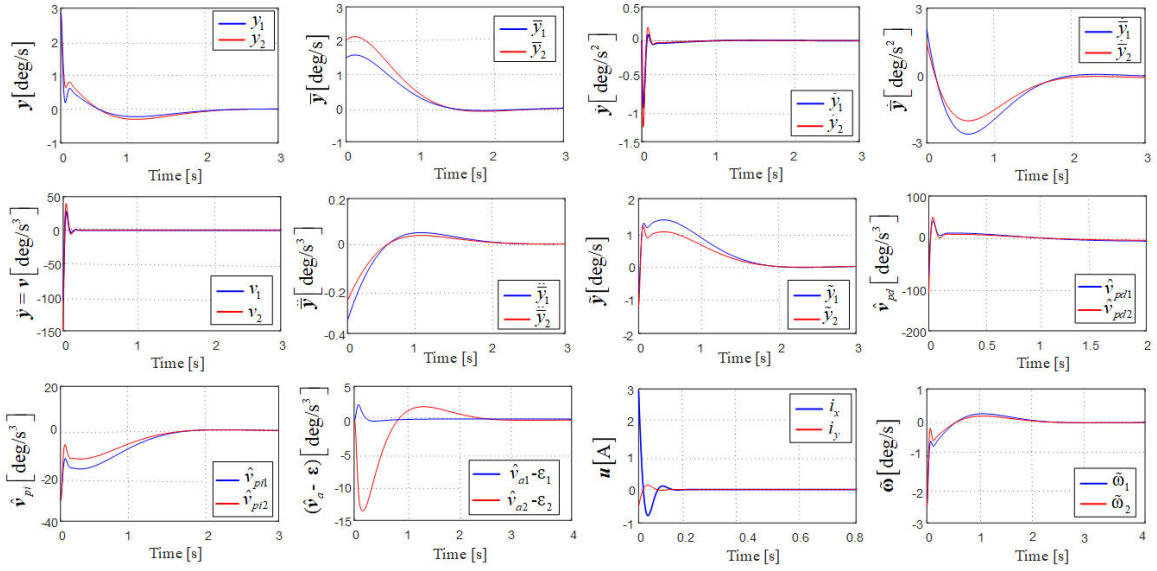

a.

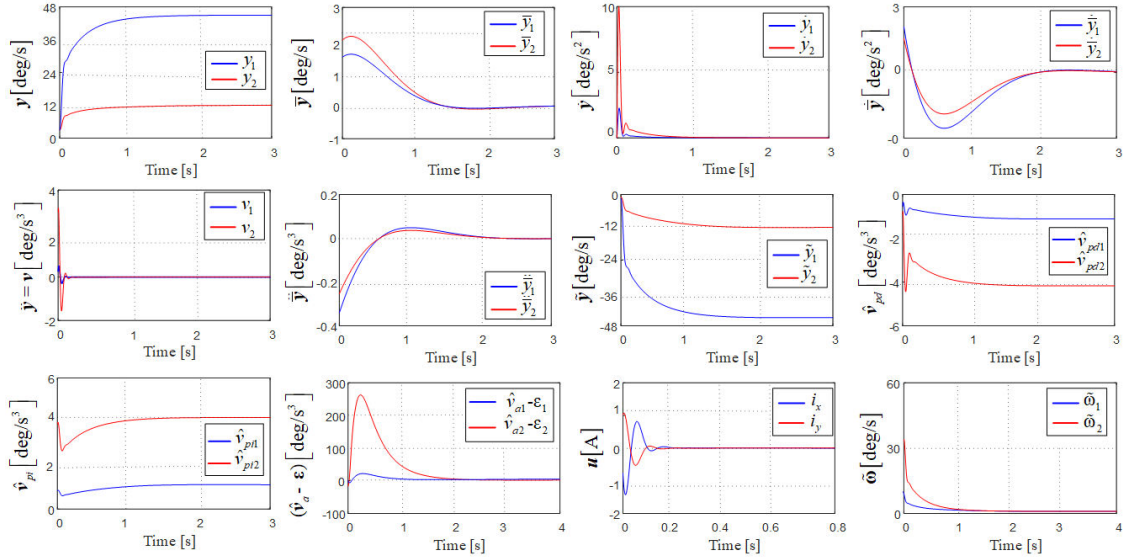

b.

FIG.3 Dynamic characteristics of the subsystems in Fig.2: a – for the stabilization mode; b – for the orientation mode

4. CONCLUSIONS

The nonlinear dynamics equations of the GG derived in Part 1 of this paper series are expressed in the form (7), with (8) and (9), and the inverse dynamics in the form (11). Using these, the system in Fig.1 was designed for the stabilization mode and for the orientation mode. The Matlab/Simulink model in Fig.2 was built and, with these, the dynamic characteristics in Fig.3 were plotted for the two operating modes.

For the stabilization mode $\bar{\boldsymbol{y}}_c = \boldsymbol{y}_c = [0\ 0]^T$ deg/s, and disturbances $N_x(t)$ and $N_y(t)$ (functions of the angular velocities of the base), are non-zero values; In orientation mode $\boldsymbol{y}_c = [\omega_{t1}\ \ \omega_{t2}\cos\lambda_2^*]^T$ and $\boldsymbol{y}_c = [0\ 0]^T$ deg/s, and $N_x = N_y = 0$.

Analyzing the dynamic characteristics of the GG in Fig.3.a and b, the following conclusions result.

Compared to linear GG, with linear control, the nonlinear ones with adaptive control based on the use of the dynamic inversion method and neural networks contain very fast dynamic regimes (under 2 seconds), with very small overshoots and stationary errors in the two regimes practically zero. Adaptive control vector quickly compensates for dynamic inversion error $(\boldsymbol{\nu}_a - \boldsymbol{\varepsilon} \to [0\ 0]^T)$ in both modes (stabilization and orientation), so that GG with nonlinear dynamics behaves very close to 2nd order linear systems.

The dynamic characteristics in Fig.3.a confirm the following:

$\boldsymbol{y} \to \overline{\boldsymbol{y}}(\tilde{\boldsymbol{y}} \to [0\ 0]^T, \dot{\boldsymbol{y}} \to \dot{\overline{\boldsymbol{y}}}(\dot{\tilde{\boldsymbol{y}}} \to [0\ 0]^T)$ and $\boldsymbol{y} = \boldsymbol{\nu} \to \boldsymbol{y} = [0\ 0]^T (\ddot{\tilde{\boldsymbol{y}}} \to [0\ 0]^T)$, $\hat{\boldsymbol{\nu}}_{pi} + \hat{\boldsymbol{\nu}}_s =$

$= \hat{\boldsymbol{\nu}}_{pi} + \hat{\boldsymbol{\nu}}_{pd} \to [0\ 0]^T$, and $\hat{\boldsymbol{\nu}}_a - \boldsymbol{\varepsilon} = [0\ 0]^T$.

So, the output $\tilde{\boldsymbol{y}}$ of the subsystem with the input $(\boldsymbol{\nu}_a - \boldsymbol{\varepsilon})$ and its derivatives tend to $[0\ 0]^T$ with the input $[0\ 0]^T$; thus $\hat{\boldsymbol{e}}$ and $\overline{\boldsymbol{e}} \to [0\ 0]^T$.

Similarly, we can say about the characteristics in Fig.3.b, with the difference that $\tilde{\boldsymbol{\omega}} \to [0\ 0]^T$ and $\tilde{\boldsymbol{y}} \to -\boldsymbol{y} = -\boldsymbol{y}_c$.

REFERENCES

[1] B. Fenu, V. Atanasio, *Analysis of gyroscopic–stabilized floating offshore hybrid wind–wave platform*, Journal of Marine Science and Engineering, 8,439, 21 pag., 2020;

[2] H. Kojima, R. Nakamura, S. Keshtkar, *Steering control low for double gimbal scissored–pair CMG*, Advance in Space Research 66, pag.771 – 784, 2020;

[3] N.C. Townesed, R.A. Shenoi, *Gyrostabilizer vehicular technology*, Transactions of the ASME, Vol. 64, 12 pag, 2011;

[4] J.D.G. Kooijman, A.L. Schwab, J.P. Meijaard, *Experimental validation of model of an uncontrolled bicycle,* Multibody Systems Dynamics, 19 pag., 2008;

[5] H. Li, S. Yang, H. Ren, *Dynamic decoupling control of DGCMG gimbal system via state feedback linearization*, Mechatronics 36, pag. 127-135, 2016;

[6] H. Li, X. Ning, B. Han, *Speed tracking control for gimbal system harmonic drive*, Control Engineering Practice, 58, pag. 204-213, 2017;

[7] S. Pan, *Robust control of gyro stabilized platform driven by ultrasonic motor. Sensor and actuators 1*, Physical A 261, pag.280 – 287, 2017;

[8] R. Lungu, M. Lungu, C. Efrim, O. Bombaker, *Backstepping control of double–gimbal control moment gyroscope*, 24 IEEE International Conference on System Teory, Control and Computing, Sinaia, România, pag. 154 – 159, 2020;

[9] M. Lungu, *Neuro-observer based control of double gimbal control moment gyro systems*, Aerospace Science and Technology, Vol. 110, 2021;

[10] M. Lungu, *Backstepping control method in aerospace engineering*, Academica Greifswald, 2022;

[11] Y. Mousavi, A. Zarei, Z.S. Jahromi, *Robust active fractional–order nonsingular terminal sliding mode stabilization of three–axis gimbal platform*, ISA Transactions 123, pag.98 – 109, 2022;

[12] B. Xiang, Q.Mu, *Gimbal control stabilized platform for airborne remote sensing systems based on adaptive RBFNN feedback Model*, IFAC Journal of Systems and Control, 16, 9 pag., 2021;

[13] Y. Zou, Xu. Lei, *A compound control method of the adaptive neural network and sliding mode control for inertial stable platform*, Neurocomputing, 155, pag.286 – 294, 2015;

[14] B. Han, Ma, Y .Chen, J. Li, Li. Ha, Li. Yang, *Discrete model reference adaptive control for gimbal servosystem of control moment gyro with harmmonic drive*, Publiching Corporation Mathematical Problems Engineering Volume, 10 pag, 2013;

[15] M.A. Thofigh, M.J. Mahjooh, M.R. Hanachi, M. Ayati, *Fractional sliding mode control for an autonomus two–wheeled vehicle equipped with an innovative gyroscopic actuator*, Robotics and Autonomous Systems 140, 9 pag., 2021;

[16] H. Kojima, R. Nakamura, S. Keshtkar, *Model predictive steering control low for double gimbal scissored–pair control moment gyros*, Acta Astronautica 183, pag. 273 – 285, 2021;

[17] S. Dey, S. Halder, M.P. Pandakumar, *Gyroscopic stabilization of two–dimensional gimbals platform using fuzzy logic control,* International Journal of Electrical and Data Communication, Vol. 2, pag.36 – 42, 2014;

[18] D.Su, S. Xu, *The precise control of double gimbal MSCMG based on modal separtion and modal separtion and feedback linearization*, International Conference on Electrical Machines and Systems, Korea, pag.1355 – 1360;

[19] R. Lungu, M. Lungu, C. Efrim, *Adaptive control of DGMSCMG using dynamic inversion and neural networks*, Advances and Space Research, Vol.68, Nr.8, pag. 3478 – 3494, 2021;

[20] Ch. Xiaocen, Ch. Maoyin, *Precise control of magnetically double gimbal control moment gyroscope using differential geometric gecoupling method*, In Chinese Journal of Aeronautics, 26(4), pag. 1017 – 1028, 2013;

[21] R. Lungu, C. Efrim, Z. Zheng, M. Lungu, *Dynamic inversion based of control of DGMSCMGs. Part 1: Obtaining nonlinear model*, IEEE International Conference on Applied and Theoretical Electricty (ICATE), pag.1 – 6, 2021;

[22] R.Lungu, M. Lungu, C. Efrim, *Attitude adaptive control of sattelites using double–gimbal magnetically suspended control moment gyros*, Aerospace Science and Technology, Vol. 126, 2022;

[23] A.J.Calise, E.N. Jonson, M.D. Jonson, J.E. Oorban, *Aplicațions of adaptive neural–networks control to unmanned aerial vehicles*, Journal of Harbin Institute of Technology, Vol.38., Nr.11, pag. 1865 – 1869, 2006;

[24] A.J. Calise, N. Hovakymyan, M. Idan, *Adaptive outpout control of nonlinear systems using neural networks*, Automatica, Vol.37, Nr.8, pag. 1201 – 1211, 2001;

[25] A. Isidori, *Nonlinear control systems*, Springher, Berlin, 1995;

[26] R. Lungu, C.A. Mihai, *Dynamic and Adaptive Control of Monoaxial GS with GAR. Part 2: Control Arhitecture Design and Validation*, IEEE International Conference on Applied and Theoretical Electricity (ICATE),pag.1 – 6, 2024.